Zhou *et al. Respiratory Research* (2025) 26:1
https://doi.org/10.1186/s12931-024-03072-x

Respiratory Research

RESEARCH Open Access

Proteomic characterization of molecular mechanisms of paraquat-induced lung injury in a mouse model

Yu Qing Zhou[1†], Jin Jin Peng[1†], Li Ping Shan[2,3†] and Wei Liu[1*]

Abstract

Background We sought to explore the molecular mechanisms underpinning acute lung injury (ALI) caused by poisoning with paraquat (PQ).

Methods Selection mice were intraperitoneally injected with PQ at 40 mg/kg, whereas controls were injected with sterile saline. On days 2, 7, and 14 after administration, mice were anesthetized and sacrificed, and lung tissue was removed. Lung pathological changes were observed with conventional staining techniques. Lung tissue components were assessed with tandem mass spectrometry tag technology, and differentially expressed proteins (DEPs) were bioinformatically analyzed and investigated with parallel reaction monitoring.

Results The expression of 91, 160, and 78 proteins was significantly altered at days 2, 7, and 14, respectively. Gene Ontology analyses revealed that the DEPs in the PQ-2d and PQ-7d groups were involved primarily in humoral immunity and coagulation-related reactions, whereas those in the PQ-14d group were implicated primarily in chemotactic and regulatory responses. Kyoto Encyclopedia of Genes and Genomes analyses indicated that complement and coagulation cascades were key pathways in the PQ-2d and PQ-7d groups, whereas xenobiotic metabolism by cytochrome P450 was a key pathway in the PQ-14d group. Nine proteins at PQ-2d and eight proteins at PQ-7d were validated through parallel reaction monitoring (PRM).

Conclusions PQ-induced ALI depends on over-activation of immune responses by damaged alveolar/endothelial cells, and the complement/coagulation cascade pathway plays a key role during this process. The proteins identified herein might provide new therapeutic targets or biomarkers for PQ poisoning.

Keywords Paraquat, Poisoning, Acute lung injury, Proteomics, Differentially expressed proteins, Complement coagulation cascades

†Yuqing Zhou, Jinjin Peng and Liping Shan are co-first authors.

*Correspondence:
Wei Liu
Dr.liuweicmu@hotmail.com
[1]Emergency Department, The First Hospital of China Medical University, No.155 North Nanjing Street, Heping District, Shenyang, Liaoning 110001, China
[2]Key Laboratory of Health Ministry for Congenital Malformation, Shengjing Hospital of China Medical University, Shenyang, Liaoning 110004, China
[3]Urology Surgery, ShengJing Hospital of China Medical University, Shenyang, Liaoning 110004, China

Background

Since the 1960s, the non-selective contact bipyridyl compound paraquat (PQ) has been extensively used as a selective herbicide and was believed to be a non-toxic agent in the environment [1]. However, the agent is extremely toxic, causing human mortality rates of 60–80% after exposure [2]. In China, although 20% PQ water solvents have been banned, PQ poisoning incidents persist; e.g., PQ poisoning suicide is a considerable global health issue, particularly in developing countries [3].

The main target organ of PQ poisoning is the lungs, and type I and II pneumatocytes selectively accumulate the agent [4]. Although the main toxicity agent of PQ is considered to be reactive oxygen species, therapeutic administration of antioxidants is largely unsuccessful in PQ-poisoned patients [5]. Several patients with PQ poisoning have undergone lung transplantation, but the curative effects were not definite, and medical costs were high [6]. DNA microarray studies have elucidated several molecular mechanisms underpinning PQ-induced lung injury [7]. Studies investigating individual proteins, e.g., metallothioneins, p38 mitogen-activated protein kinase, and endocan [8–10], in PQ-induced lung injuries have also been reported. However, understanding of the exact mechanisms underlying PQ-induced lung injury remains limited, and more precise studies are required.

Proteomics is a frequently used method for investigating disease molecular mechanisms, new diagnostic markers, and therapeutic targets [11, 12]. In contrast to traditional single protein approaches, proteomics accurately quantifies and identifies all expressed proteins in a genome or complex system. Notably, recent research studies have incorporated tandem mass tag (TMT) and high-performance liquid chromatography tandem mass spectrometry (LC-MS/MS) methods into proteomic-based qualitative and quantitative analyses [13, 14]. Some studies have used proteomics to explore the protein changes in the lung, heart, and liver in animal models (in mice or rats) of PQ poisoning [15–17]. However, no consecutive time-course study has been conducted, because diverse manifestations of lung injury are observed across stages of PQ poisoning. Clinical mortality is associated primarily with lung injury; therefore, proteomics of lung tissues is important for understanding and treating PQ poisoning. Here, we conducted a time-course proteomics analysis by using TMT to monitor PQ-induced protein expression alterations in lung tissues in a mouse model. Parallel reaction monitoring (PRM) was also performed to confirm the MS data. Our results provide information for designing novel diagnostic and therapeutic interventions.

Materials and methods

Mouse models and sample collection

C57BL/6 male mice (N=50, 6–8 weeks of age and weighing 18–22 g) were obtained from the animal laboratory at China Medical University, China. The animals were given free access to standard chow and water for 7 days before the studies. The controlled rearing conditions were as follows: 12 h light/dark cycle, 23 °C±0.5 °C temperature, and 50% ± 5% humidity. Selected mice (N=40) were intraperitoneally injected with PQ (St. Louis, MO, USA) at 40 mg/kg in sterile saline [18], whereas controls (N=10) received sterile saline. At days 2, 7, and 14 after PQ administration, nine mice at each time point, as well as control mice, were anesthetized (pentobarbital, 60 mg/kg), Sigma-Aldrich) and sacrificed. Subsequently, the heart and lungs were exposed, the abdominal aorta was cut, and warm saline was perfused under constant pressure from the right ventricle through the pulmonary circulation until the lungs became white. The lungs were then removed. The left lung was stored at -80 °C. The right lung was cut in two, and the upper lobe was immersed in 10% neutral buffered formalin and paraffin-embedded for hematoxylin and eosin (H&E) staining, whereas the lower lobe was frozen at -80 °C. All animal experiments were performed in accordance with the National Institutes of Health Guide for the Care and Use of Laboratory Animals (NIH Publications No. 8023, revised 1978).

Histology

Lung tissues were routinely treated with formaldehyde, paraffin-embedded, cut into 5 μm sections, stained in H&E, and observed with optical microscopy (Nikon, Japan, ×100). Stained lung sections were evaluated in a blinded fashion by two experienced pathologists. Lung tissue pathology scoring was performed according to a previous study, and the resulting injury score was determined as a continuous value between 0 and 1 [19].

Extraction and digestion of proteins

Ultrasonic crushing (10 s ultrasonication and 15 s pause, for ten cycles) was used to grind the lung tissues. The lung tissues were placed into a 1.5 ml centrifuge tube, to which 200 μl SDT buffer (4% SDS, 100 mM Tris-HCl, and 1 mM DTT, pH 7.6) was added to lyse the samples. The samples were immersed in a boiling water bath for 5 min and centrifuged for 20 min (25℃, 2000 g), and the supernatant was collected. A bicinchoninic acid protein assay kit was used to quantify proteins (Bio-Rad, USA), which were subsequently digested in trypsin with a filter-aided sample preparation protocol [20]. After digestion, peptides were desalted with C18 cartridges (Empore™ SPE Cartridges C18 (standard density), bed inner diameter=7 mm, volume=3 ml, Sigma-Aldrich, MO USA),

concentrated by vacuum centrifugation, dissolved in 40 µl 0.1% (v/v) formic acid, and quantified at 280 nm with a spectrophotometer (Thermo Multiskcan FC).

TMT labeling

TMT technology is an ex vivo peptide labeling technique. In this experiment, we used TMT labeling to mark peptide mixtures to quantify the protein levels across sample groups. Specifically, 100 mg peptides from each sample was labeled with TMT reagents from Thermo Fisher Scientific. The four experimental groups comprised a control group, PQ-2d group, PQ-7d group, and PQ-14d group. Each group included three biological replicates (each comprising a mixture of three independent samples), thus resulting in a total of 12 samples. This TMT labeling allowed us to track and compare protein expression across conditions in a single mass spectrometry analysis.

Strong cation exchange fractionation of proteins

In this step, we used strong cation exchange chromatography to separate the labeled peptides into fractions, to facilitate the analysis of complex peptide mixtures. We prepared the peptide samples in acidic buffer A (10 mM KH_2PO_4 in 25% acetonitrile (ACN), pH 3.0) and loaded them onto a PolySULFOETHYL 4.6×100 mm column (5 µm, 200 Å, PolyLC Inc, Maryland, USA) designed to capture positively charged molecules. Peptides were gradually eluted by changing the concentration of buffer B (500 mM KCl, 10 mM KH_2PO_4 in 25% ACN, pH 3.0). Peptides were eluted at 1 ml/min in buffer B through a gradient as follows:

- Only buffer A (0% buffer B) for the first 25 min.
- Gradual increase of buffer B from 0 to 10% from 25 to 32 min.
- Continued increase to 20% buffer B between 32 and 42 min.
- Increase to 45% buffer B from 42 to 47 min.
- Increase to 100% buffer B from 47 to 52 min.
- Hold at 100% buffer B for 8 min (52 to 60 min).
- Reset to 0% buffer B after 60 min.

Peptide elution was monitored according to the absorbance at 214 nm, and fractions were collected every 60 s. These fractions were later desalted and prepared for mass spectrometry analysis. This method enabled simplification of the complex mixture, thus facilitating protein identification and quantification.

Liquid chromatography tandem mass spectrometry data acquisition

LC-MS/MS analysis was performed with a Q Exactive mass spectrometer (Thermo Fisher Scientific) coupled with an Easy nLC liquid chromatography system (Thermo Fisher Scientific). The analysis run lasted for 90 min, the total time for separating and identifying peptides in the sample. Peptides (small protein fragments) were first loaded onto a trap column (Thermo Scientific Acclaim PepMap100, 100 µm × 2 cm), which was used to concentrate the peptides before separation. Subsequently, the peptides were transferred to an analytical column (Thermo Scientific EASY column, 10 cm × 5 µm, filled with C18 resin to separate peptides according to their properties). Buffer A (0.1% formic acid), the starting solution, helped keep the peptides in solution. Buffer B was used to elute the peptides off the column in a gradient of increasing ACN concentration (84% ACN and 0.1% formic acid). The flow rate of the solution was controlled at a very low rate of 300 nL/min, as managed by an IntelliFlow system for precise delivery. The MS was set to detect positively charged ions and used a "top ten" method selecting the ten most abundant ions from each survey. These ten ions were then analyzed in greater detail to understand their structure. The survey scan ranged from a mass-to-charge ratio of 300 to 1800 m/z, to capture the full range of peptides. High energy collisional dissociation was used to break the ions into smaller fragments for further analysis.

The automatic gain control was set to 3e6; i.e., the MS accumulated a target of 3 million ions before starting the analysis. The maximum injection time, the time during which ions were allowed to accumulate before MS analysis, was set at 50 ms. Dynamic exclusion was set to exclude ions detected multiple times from the next scans for 60 s, to avoid redundancy in the data. The resolution indicates how finely the MS can distinguish between ions with different m/z values. Survey scans were acquired at a very high resolution of 70,000 at 200 m/z (enabling accurate differentiation of ions very close in mass). High energy collisional dissociation spectra were acquired at a slightly lower resolution of 17,500 at 200 m/z. The isolation width for fragmentation was set to isolate ions within a 2 m/z range, thus ensuring that only the most relevant ions were fragmented. Normalized collision energy, the amount of energy used to break the ions, was set at 30 eV, to provide sufficient energy to fragment the ions without over-dissociating them. The underfill ratio, the percentage of the maximum ion capacity required to be filled during the MS acquisition, was set to 0.1%; i.e., the MS only acquired data when it's nearly full, thereby avoiding wasted time. The system was set to automatically identify peptides during the analysis. This aspect was essential for our proteomic analysis, wherein large datasets were generated. Peptide identification was crucial for understanding the protein content of the sample.

Identifying and quantifying proteins

For identification and quantification analyses, MS raw sample results were investigated with MASCOT (Matrix Science, London, UK; version 2.2) embedded in Proteome Discoverer 1.4 software. Related factors/instructions are outlined in the Supplementary Table. All raw files were searched against the Universal Proteins Resource Knowledgebase (UniProt, www.uniprot.org) protein database.

Bioinformatics analyses

Cluster analyses

We used Cluster 3.4 and Java Treeview to perform hierarchical clustering on our data. To measure similarity between data points, we chose the Euclidean distance. For the clustering algorithm, we used the average linkage; i.e., we considered the average similarity between all points in the clusters. The results were visualized with a dendrogram to demonstrate how the data points were grouped by similarity, and a heatmap was generated to further support the interpretation of the clustering patterns. This process provided understanding of how the observations were grouped on the basis of underlying similarities.

Subcellular localization

Subcellular localization refers to the specific location within a cell where a protein performs its function. Understanding where a protein is located within the cell is crucial for understanding its role in cellular processes. CELLO is a software system that uses machine learning to predict the subcellular localization of proteins [21]. Here, we used the machine learning system -Support Vector Machine to help uncover potential biological roles of proteins according to their predicted localization within the cell—a key step for understanding cellular mechanisms.

Domain annotation

Protein domains—distinct functional and structural units within a protein—are often responsible for specific functions or interactions with other molecules in the cell. Each domain can be considered a "module" within the protein, which contributes to the protein's overall structure and function. Domains often correlate with specific biological activities. Understanding the domain composition of a protein can importantly reveal insights into a protein's function, potential interactions, and involvement in cellular processes. InterProScan is a widely used bioinformatics tool for analysis of protein sequences for domain signatures, functional sites, and other features, through comparison against multiple protein family and domain databases. Pfam, one of the most well-known databases of protein families and domains, contains a large collection of sequence alignments for thousands of protein families and functional domains. We used InterProScan to search for protein domains within the protein sequences to identify potential functional domains.

Gene Ontology annotations

Sequences from selected differentially expressed proteins (DEPs) were processed with National Center for Biotechnology Information Basic Local Alignment Search Tool (BLAST)+client software (ncbi-blast-2.2.28+-win32.exe) and InterProScan to detect homologous sequences. Gene Ontology (GO) terms were then mapped, and sequences were annotated with Blast2GO (Version 3.3.5). GO annotation results were plotted with R scripts. We used Blast2 GO software [22] to annotate DEP GO functions. Fisher's exact tests were used to determine the overall functional enrichment characteristics of DEPs and the significantly enriched GO terms.

Kyoto Encyclopedia of genes and genomes annotation

After annotation, proteins were analyzed with the Kyoto Encyclopedia of Genes and Genomes (KEGG) database to retrieve KEGG orthologs and were mapped to KEGG pathways.

Enrichment analyses

Enrichment analyses were based on Fisher's exact tests. Benjamini-Hochberg correction for multiple testing was used to adjust p-values. GO enrichment was determined with the following terms: molecular function (MF), biological process (BP), and cellular component (CC). KEGG pathway analyses were performed with Fisher's exact tests, with quantified protein annotations as the basic dataset. Functional categories and pathways with P-values < 0.05 were considered statistically significant.

PPI analyses

We retrieved PPI information from the IntAct molecular interaction database with gene symbols, or the Search Tool for the Retrieval of Interacting Genes/Proteins (STRING) software (http://string-db.org/). Results were downloaded in XGMML layout and transferred to Cytoscape software (version 3.2.1) to process PPI networks. The degree of each protein was calculated to estimate its importance in the PPI network.

PRM analyses

To determine protein expression levels from TMT analyses, we performed additional quantification analyses with liquid chromatography-parallel reaction monitoring/mass spectrometry [23]. We used the TMT protocol to prepare peptides. Samples were spiked with the isotopically labeled AQUA standard internal peptide. Tryptic peptides were loaded onto a C18 desalting column for

desalting before reverse-phase chromatography on an Easy nLC-1200 system (Thermo Scientific). Subsequently, LC gradients were run in 5–35% ACN for 45 min, and Q Exactive Plus MS was used for PRM. Unique peptides with high intensities were selected to determine the collision energy, the charge state, and key peptide retention times for each targeted protein. Signal intensities from specific peptide sequences were quantified with respect to each sample and normalized to reference standards for each protein. Skyline software [24] (MacCoss Lab, University of Washington, USA) was used to analyze the raw data and quantify protein expression levels (Fig. 1).

Statistical analysis

Statistical analysis was performed in SPSS Statistics 21.0 (SPSS, Inc., Chicago, IL, USA). The significance of differences between two groups was assessed with two-tailed Student's *t*-tests, and a P-value <0.05 was considered statistically significant.

Results

Pathological alterations in the lung

Intraperitoneal injection of PQ is used to elicit PQ induced lung injury in mouse models [25]. After PQ intraperitoneal injection, eight mice in the experimental groups died: three at day 2, two at day 4, and three at day 7. These deaths suggested that early acute lung injury (ALI) stages (within 7 days) led to a high incidence of death. H&E staining in PQ-2d mice, compared with controls, showed alveolar structure destruction, hemorrhaging in alveolar cavities, and inflammatory cell infiltration. Alveolar structure destruction in the PQ-7d group was further aggravated by thickening of the local alveolar septum, diffuse hemorrhaging, and inflammatory cell infiltration. In PQ-14d mice, the alveoli lost their normal structures and showed thickened alveolar walls. The significantly higher lung pathology scores in the PQ groups than the control group indicated that the mouse model of PQ induced ALI was successfully established (Fig. 2).

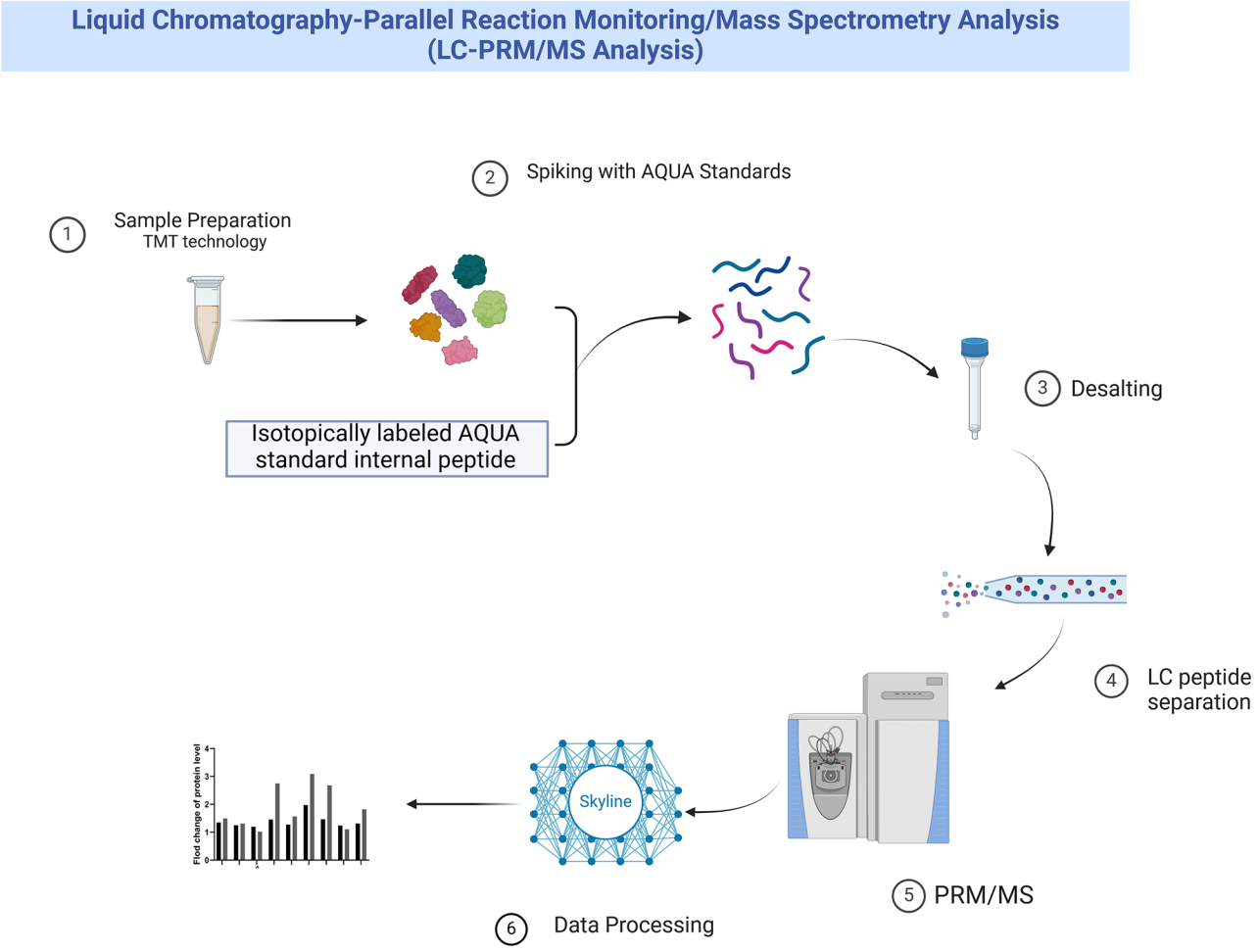

Fig. 1 Liquid Chromatography-Parallel Reaction Monitoring/Mass Spectrometry Analysis workflow. (Created in https://BioRender.com)

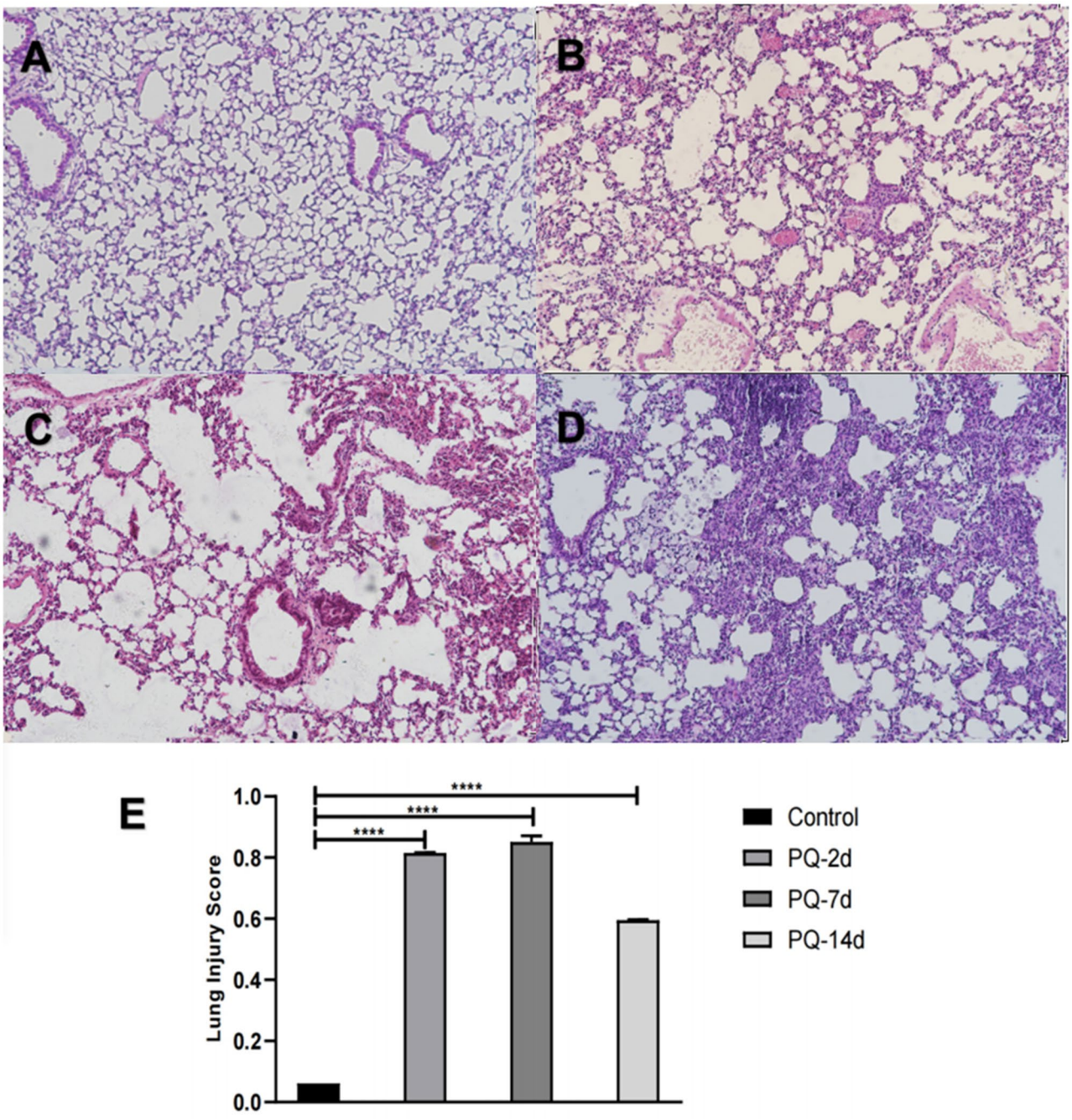

Fig. 2 Lung tissue staining with Hematoxylin & Eosin (× 100 magnification). (**A**) Control tissue, (**B**) PQ-2d tissue (**C**), PQ-7d tissue, (**D**) PQ-14d tissue, and (**E**) Lung injury score. *$P < 0.05$, **$P < 0.01$, ***$P < 0.001$, ****$P < 0.0001$ compared to control group

LC-MS/MS data

MS identified 89,554 peptide fragments; 80,215 were single peptide fragments, whereas 6973 were corresponding proteins (Fig. 3). Fold DEP changes were identified as intergroup ratios from TMT data. Proteins conforming to the following screening criteria were considered DEPs: expression fold change > 1.2 (up- or down-regulated) and P-value < 0.05. PQ-2d/control, PQ-7d/control, and PQ-14d/control comparisons identified 91 (69 up- and 21 down-regulated), 160 (103 up- and 57 down-regulated), and 78 (45 up- and 33 down-regulated) DEPs, respectively (Fig. 4, Supplementary File). Thus, DEPs were primarily up-regulated during PQ-induced lung injury, and were most significantly expressed at day 7.

Cluster analyses

By applying our screening criteria, we determined that significant DEPs effectively distinguished the comparison

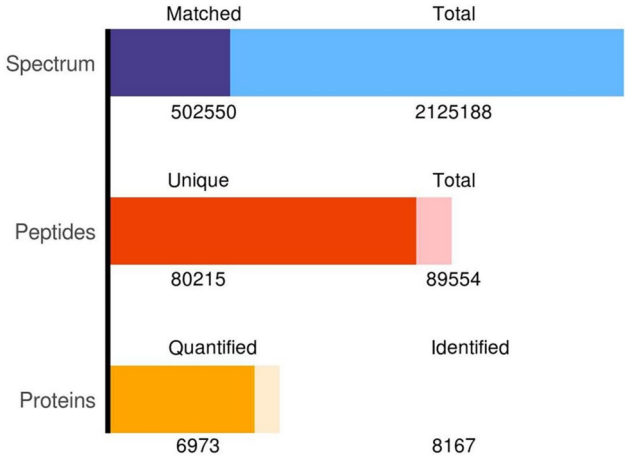

Fig. 3 Bar graph shows the identified results of LC-MS/MS data

groups (Fig. 5A–C), thus suggesting that our strategy robustly reflected the effects of PQ on mice (Supplementary File).

Subcellular localization analyses

The mitochondria and endoplasmic reticulum are organelles with unique cytoplasmic functions. Because these subcellular organelles perform different cellular functions, protein subcellular localization can help determine protein function in cells. Most PQ-2d DEPs with respect to the control were located outside the cell, followed by the nucleus and cytoplasm. Some DEPs were distributed on the cell membrane and mitochondria, and the fewest DEPs were distributed in lysosomes. In the PQ-7d group, most DEPs with respect to the control were distributed outside the cell, followed by the cytoplasm and then the nucleus. Some DEPs were located on the cell membrane, mitochondria, and endoplasmic reticulum, and the fewest DEPs were located in lysosomes. In the

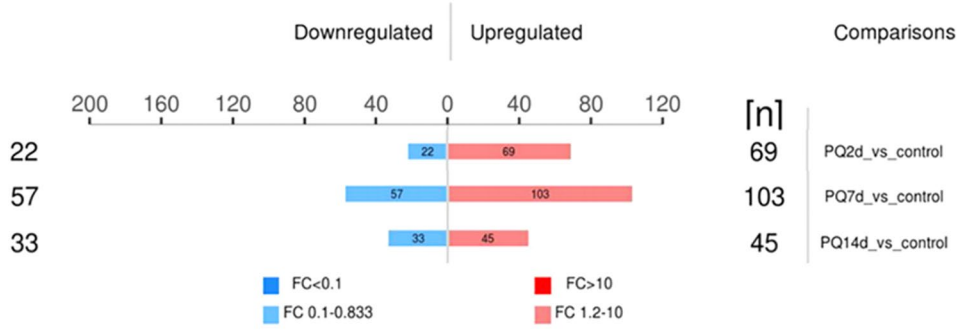

Fig. 4 Differentially expressed proteins (DEPs) in different groups when compared with controls. Red = up-regulated and blue = down-regulated proteins

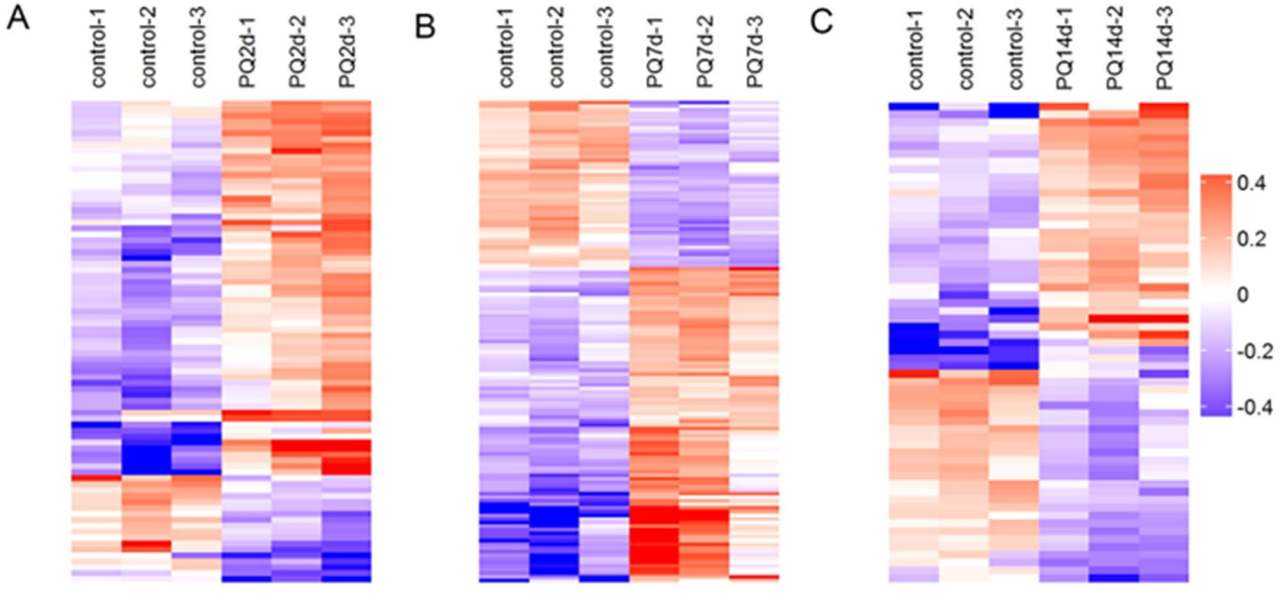

Fig. 5 Hierarchical clustering of differentially expressed protein (DEP) abundance changes. Using horizontal comparisons, samples were assigned to three categories meaning that DEPs effectively distinguished samples. Vertical comparisons meant proteins could be assigned to two categories with opposite directional variations demonstrating the rational choice of DEPs. (**A**) PQ-2d/controls, (**B**) PQ-7d/controls, and (**C**) PQ-14d/controls

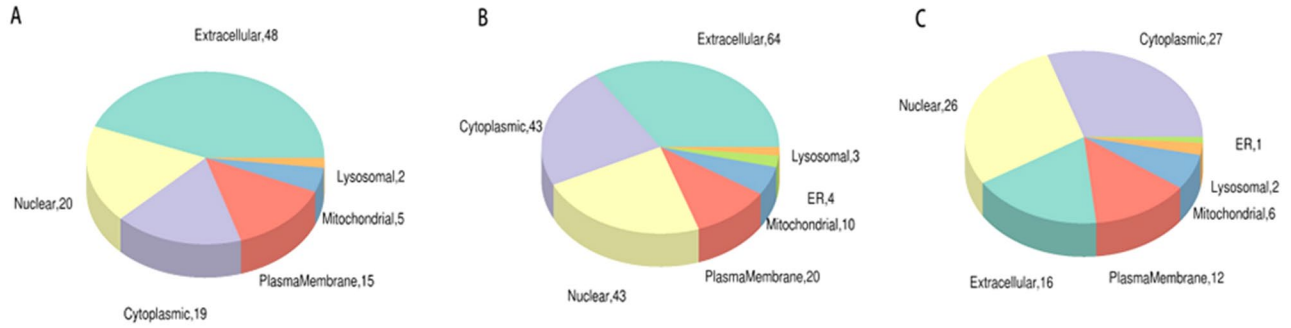

Fig. 6 Pie chart showing subcellular localization of differentially expressed proteins (DEPs) in groups compared to controls. (**A**) PQ-2d/controls, (**B**) PQ-7d/controls, and (**C**) PQ-14d/controls

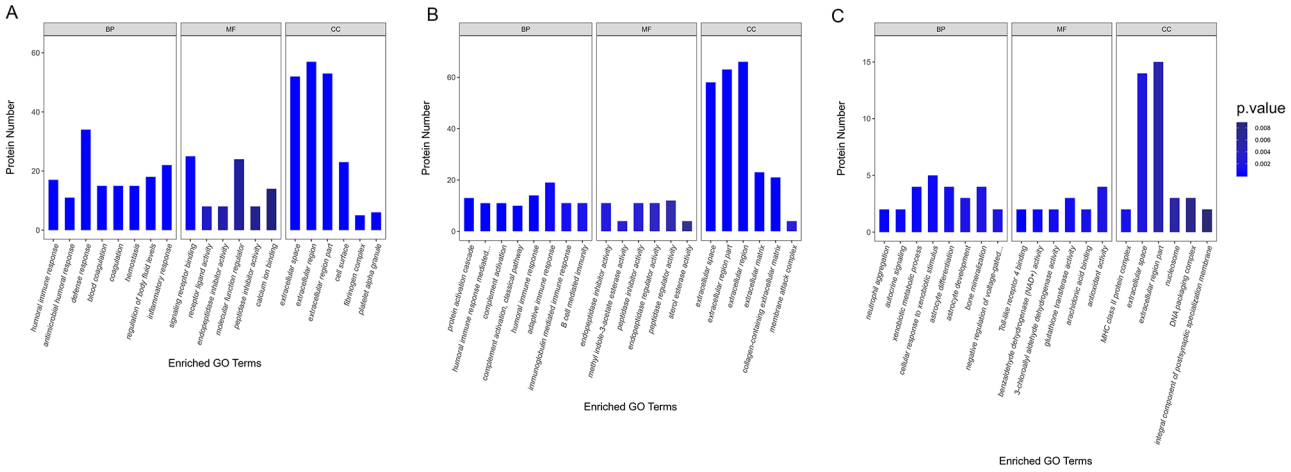

Fig. 7 Gene ontology (GO) functional annotations (BP, MF and CC) and differentially expressed protein (DEP) analysis. Abscissa displaying Top 20 GO terms in comparison groups and ordinate showing the protein numbers in each GO term. (**A**) PQ-2d/controls, (**B**) PQ-7d/controls, and (**C**) PQ-14d/controls

PQ-14d group, with respect to the control, most DEPs were located in the nucleus, followed by extracellular spaces and then the cytoplasm. The DEP distribution on cell membranes was lowest in the PQ-14d group, as compared with the PQ-2d and PQ-7d groups (Fig. 6A–C, Supplementary File). Thus, spatial changes in DEPs after PQ induced lung injury gradually transitioned from extracellular to cytoplasmic to nuclear spaces in a time-dependent manner.

GO functional annotation and analyses

In organisms, annotating proteins with GO terms enhances understanding of protein function, localization, and biological pathways. Terms are classified as MF, CC, and BP. Compared with controls, PQ-2d mice displayed significant differences in the BP in terms of humoral immune responses, antimicrobial humoral responses, defense responses, blood coagulation, and coagulation (Fig. 7, Supplementary File). For MF, significant differences were observed in signaling receptor binding, receptor ligand binding, endopeptidase inhibitors, molecular function regulation, and peptidase inhibitors. Finally for CC, significant differences were observed in extracellular spaces, extracellular regions, extracellular region parts, cell surfaces, and fibrinogen complexes (Fig. 7A, $P<0.05$).

PQ-7d mice and control mice displayed significant differences in BP, in terms of protein activation cascades, humoral immune responses induced by circulating immunoglobulins, complement activation pathways, complement activation classical pathways, humoral immune responses, adaptive immune responses, immunoglobulin mediated immune responses, and B cell mediated immunity. For MF, significant differences were observed in endopeptidase inhibitor activity, methyl indole-3-acetate esterase activity, and peptidase inhibitor activity. Finally for CC, significant differences were observed in extracellular spaces, extracellular region parts, and extracellular regions (Fig. 7B, $P<0.05$).

PQ-14d mice, compared with controls, displayed significant differences in BP, in terms of neutrophil aggregation, autocrine signaling, and xenobiotic metabolic processes. For MF, significant differences were observed in Toll-like receptor 4 (TLR-4) binding, benzaldehyde dehydrogenase activity, and 3-chloroallyl aldehyde dehydrogenase activity. Finally, significant differences were observed in CC for major histocompatibility

complex (MHC) class II protein complexes and extracellular spaces (Fig. 7C, $P<0.05$). Thus, humoral immune responses and coagulation related reactions predominated in early PQ-induced lung injury stages (PQ-2d and PQ-7d).

KEGG pathway analyses

Protein expression changes were evaluated on the basis of protein annotations in the KEGG database, to systematically and comprehensively analyze biological processes, disease mechanisms, and drug action mechanisms. All DEPs were annotated to KEGG pathways (Supplementary File), and those in the same pathway were counted. A total of 115 KEGG pathways were matched to 91 DEPs in PQ-2d mice, compared with controls, of which 14 pathways were significantly affected by PQ treatment ($P<0.05$). Complement and coagulation cascades, *Staphylococcus aureus* infections, chemokine signaling, the phagosome, and platelet activation displayed the highest numbers of DEPs. Enrichment analyses indicated significant differences between these groups for complement and coagulation cascades, *S. aureus* infections, interleukin-17 signaling, systemic lupus erythematosus, and intestinal immune networks producing IgA, particularly complement and coagulation cascades (P01027, Q8K0E8, P20918, Q8VCM7, E9PV24, P01029, Q61247, P20352, and Q64695 were identified as DEPs in this pathway) (Fig. 8A).

The 160 significant DEPs in PQ-7d mice (compared with controls) matched 164 KEGG pathways, of which 23 were significantly affected by PQ exposure. Complement and coagulation cascades, cancer pathways, fluid shear stress and atherosclerosis, drug metabolism–other enzymes, and *S. aureus* infections displayed the highest numbers of DEPs. Enrichment analyses indicated that complement and coagulation cascades, *S. aureus* infection, drug metabolism—cytochrome P450, and drug metabolism—other enzymes showed significant differences between these groups. Again, complement and coagulation cascades were significantly affected by PQ. These groups exhibited the highest number of significant DEPs (P22599, P07758, P32261, Q8BH35, P20918, Q8VCM7, Q8VCG4, P06684, O08677, Q61247, Q8K182, P49182, Q61129, and P14106 were DEPs in this pathway) (Fig. 8B).

In PQ-14d mice, compared with controls, 78 significant DEPs were matched to 97 KEGG pathways, of which 13 were significantly affected by PQ treatment. Xenobiotic metabolism by cytochrome P450, cancer pathways, drug metabolism—cytochrome P450, drug metabolism—other enzymes, and alcoholism displayed the highest DEP numbers. Enrichment analyses revealed and that xenobiotic metabolism by cytochrome P450, drug metabolism—cytochrome P450, and chemical carcinogenesis showed significant differences between these groups, particularly xenobiotic metabolism by cytochrome P450 (P33267, P30115, P47739, P10648, and O35660 were identified as DEPs in this pathway) (Fig. 8C). Thus, complement and coagulation cascades have key roles in early stages of PQ-induced lung injury (PQ-2d and PQ-7d), whereas xenobiotic metabolism by cytochrome P450 is important in late stages (PQ-14d).

PPI analysis

We used Cytoscape software to construct a PPI network diagram for DEPs in comparison groups, on the basis of the STRING and IntAct databases (Fig. 9A–C). Generally, higher connectivity indicates that a protein is more important to the system when it changes, and greater likelihood that a protein has important functions in preserving system balance/stability. The degree of connectivity of each DEP in different groups in the PPI network (Supplementary File) and original PPI images (Fig. S1) are shown.

PRM verification

Complement and coagulation cascades were found to be highly relevant in ALI induced by PQ in the early (2 d and 7 d) stages after PQ exposure. Thus, protein exploration in these pathways might potentially identify mechanisms, early intervention targets, or biomarkers for PQ-induced ALI. From the PPI data, we selected 20 proteins for PRM validation, including DEPs in complement and coagulation cascade pathways and closely related DEPs. Importantly, when PRM analyses and MS data indicated similar trends, the proteomic data were considered robust and credible. Nine proteins at day 2 and eight proteins at day 7 were validated with PRM (Fig. 10). At day 2 after PQ exposure, complement C3 (C3, P01027), complement C4-B (C4-B, P01029), serine protease inhibitor A3N (Q91WP6), serine protease inhibitor A3M (Q03734), β-2-glycoprotein-1 (Q01339), thrombospondin-1 (P35441), antithrombin-III (P32261), fibrinogen γ-chain (Q8VCM7), and plasminogen (P20918) were highly expressed.

At day 7, complement factor I (Q61129), complement C5 (C5, P06684), kininogen-1 (O08677), antithrombin-III (P32261), fibrinogen γ-chain (Q8VCM7), plasminogen (P20918), hemopexin (Q91×72), and serotransferrin (Q921I1) were highly expressed.

In addition, fibrinogen γ-chain, antithrombin-III, and plasminogen were highly expressed on days 2 and 7. Detailed PRM results (Supplementary File) are shown.

Discussion

We used TMT and LC-MS/MS strategies to systematically process protein expression data in PQ-poisoned mice lungs at various time points. PRM was also used to

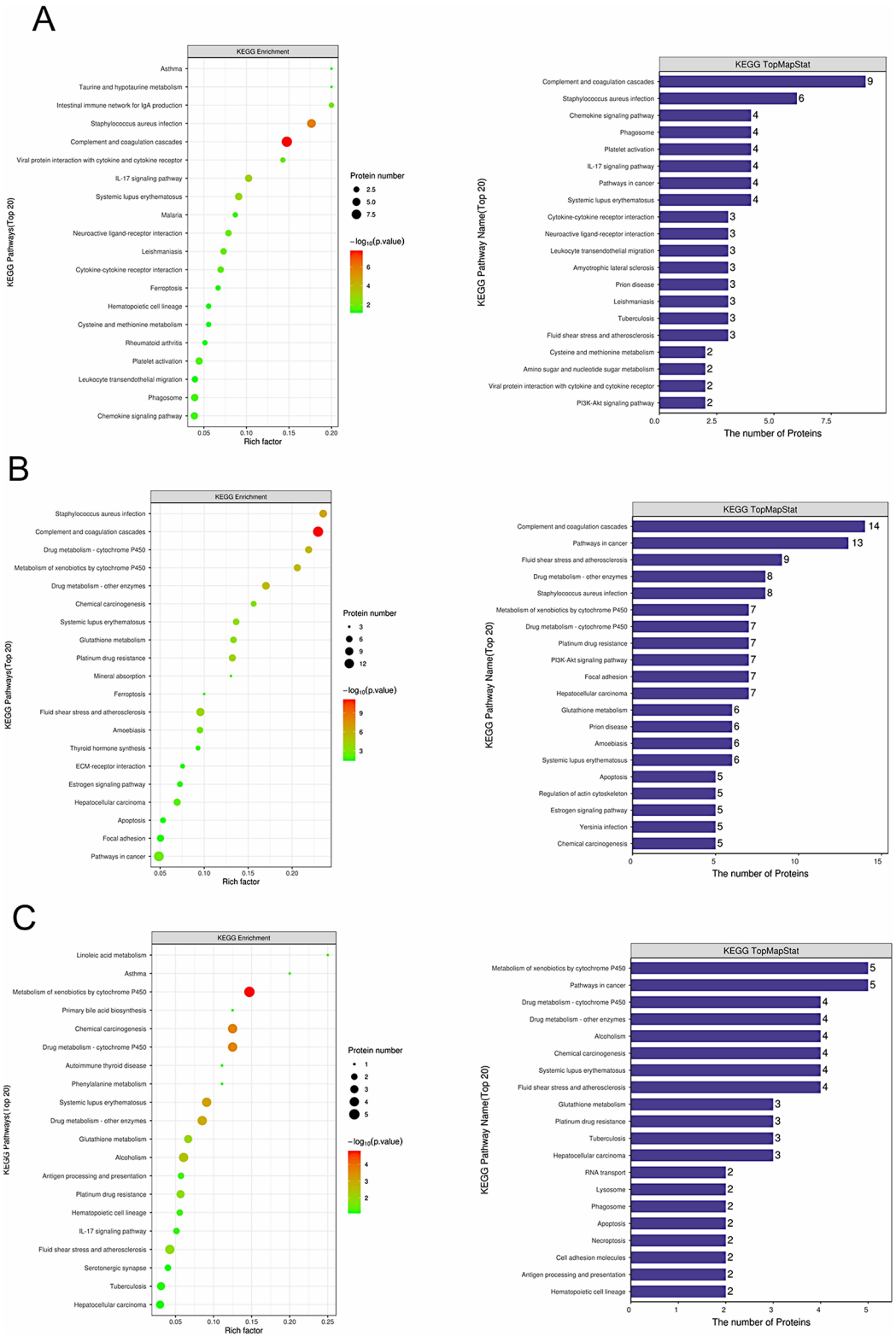

Fig. 8 Kyoto Encyclopedia of Genes and Genomes (KEGG) pathway analyses of differentially expressed proteins (DEPs). Bubble diagram shows KEGG pathway with top 20 enrichment and a bar graph shows KEGG pathway with top 20 DEP numbers when compared with control group. The more redder and bigger, the more significance the pathway is. (**A**) PQ-2d/controls, (**B**) PQ-7d/controls, and (**C**) PQ-14d/controls

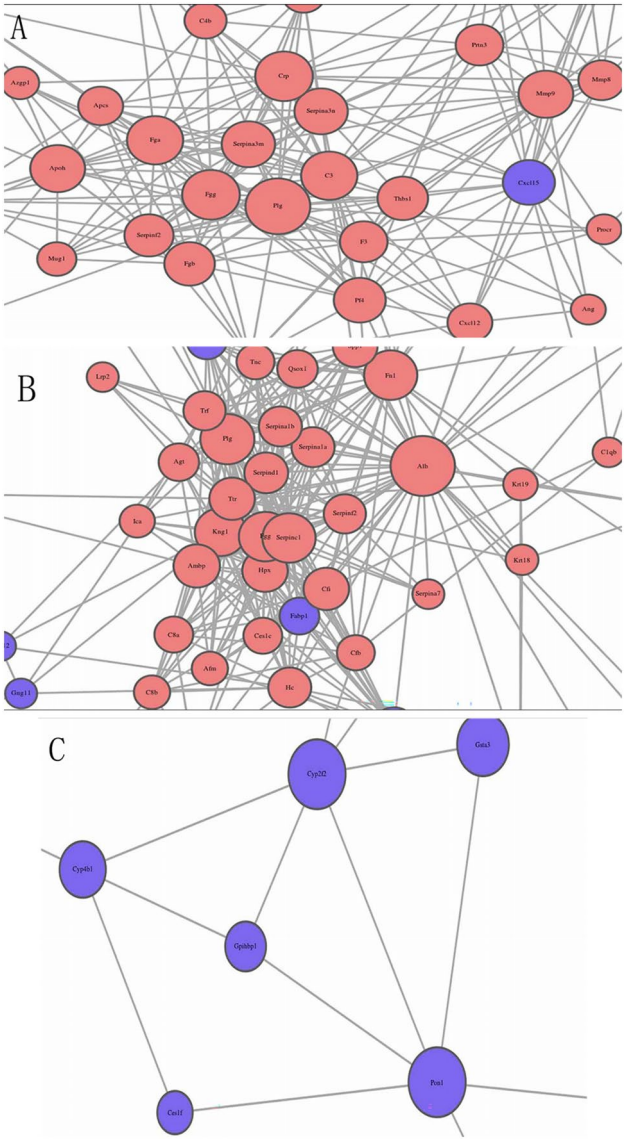

Fig. 9 Protein-protein interaction (PPI) evaluations of differentially expressed proteins (DEPs). The enlarged screenshot shows the PPIs of each comparison group. Blue = down-regulated DEPs and red = up-regulated DEPs. Circle size = protein connectivity. (**A**) PQ-2d/controls, (**B**) PQ-7d/controls, and (**C**) PQ-14d/controls

identify key regulatory proteins during ALI. We identified significant protein expression changes at various ALI stages, and importantly gained key molecular insights into PQ-induced lung injury mechanisms.

First, GO analyses (Fig. 7) revealed that humoral immune responses had key roles on days 2 and 7. PQ, in contrast to acute respiratory distress syndrome caused by bacteria or viruses, induced elevated damage-associated molecular patterns after different exposures. These patterns are recognized by immune cell surface receptors (e.g., TLRs and nucleotide-binding oligomerization domain-like receptors), which initiate pro-inflammatory and immune responses [26–28]. However, whether alveolar epithelial injury is a primary effect of PQ insult or is secondary to lung endothelial injury remains unknown. Although the alveolar epithelium can take up PQ, this is more likely the entry point. Previous research has indicated that after a lethal oral PQ dose, patients with human immunodeficiency virus could be cured, even without interventional treatment [29–31]. Although the precise mechanisms are unclear, the predominant immunological trait of patients with human immunodeficiency virus is the absence of a fully functioning immune system; therefore, effective immune responses cannot initiate when tissues are damaged [32]. This evidence suggests that an endogenous immune overreaction might be a major cause of PQ mediated ALI.

KEGG analyses demonstrated that complement and coagulation cascades displayed the most significant differences at days 2 and 7 after PQ poisoning. In addition, the numbers of DEPs were highest in these pathways. Considering the importance of coagulation cascade pathways, we verified the DEPs with PRM. We determined that expression of C3 and C4-B significantly increased at day 2, and that of complement factors I and C5 increased significantly at day 7. Complement, a key component of the humoral immune system, is activated after attack by foreign agents or pathogens [33]. Notably, complement activation not only provides rapid protection from infectious challenges but also drives pathophysiology in many inflammatory or autoimmune diseases, such as sepsis, ischemic stroke, cancer, and age-related neurodegenerative diseases [32, 34, 35]. Complement C3c, complement C3a, complement C5a, and complement C5b-9 are important activation markers that have been used to evaluate treatment effectiveness and prognosis in ALI/acute respiratory distress syndrome [36, 37]. Complement is activated not only in extracellular environments but also at various intracellular locations [38]. In patients, primates, and mouse models with ALI induced by PQ poisoning, plasma C3a and C5a (extracellular) inhibition significantly decreases abnormal complement activation and cytokine storms [36, 37]. C3 intracellular activation has also been observed in B cells, monocytes, fibroblasts, $CD4^+$ T cells, and endothelial and epithelial cells [39, 40]. In our study, C3, C4-B, and C5 expression increased in intracellular spaces (Fig S2), thus suggesting that intracellular complement activation plays essential roles during PQ poisoning. In addition, C3 appears to be a vanguard molecule whose expression significantly increased on day 2 after PQ poisoning. According to KEGG analyses (Supplementary File), classical, lectin and alternative complement pathways are all involved in these processes. Recently, intracellular C3 has been shown to protect human airway epithelial cells against stress-associated death and might have important ramifications in COVID-19 [41]. Thus, the investigation of key

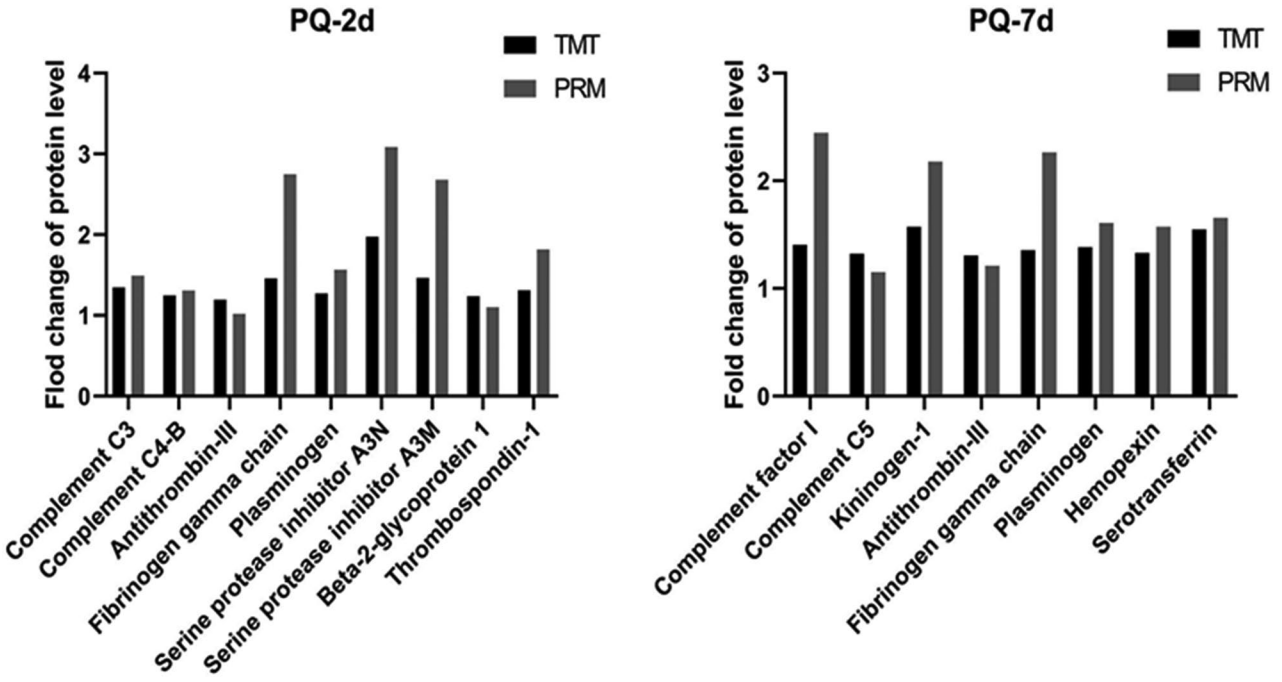

Fig. 10 Parallel reaction monitoring (PRM) verification of selected proteins. When PRM analyses showed similar trends to MS data (TM), this indicated robust and credible proteomic data. Nine proteins at day 2 and eight at day 7 after PQ exposure were validated by PRM

complement components, including C3 and C5, provides clear insights into disease pathogenesis and potentially generates promising targeted therapies for PQ-induced lung injury. We also observed that extracellular complement factor I expression increased at day 7 after PQ poisoning, and KEGG analyses indicated that this protein inhibits C3 activity. Further study is necessary to determine whether elevated complement factor I expression self-limited complement over-activation at this stage.

Our PRM analyses verified that fibrinogen γ-chain, plasminogen, and antithrombin-III in the coagulation pathway significantly increased at days 2 and 7 after PQ poisoning. In addition, kininogen-1 increased at day 7, thus suggesting that both endogenous and exogenous coagulation pathways were simultaneously activated. As indicated in the KEGG map (Fig S2), the exogenous coagulation pathway was activated by tissue factor (TF), whereas the endogenous pathway was activated by plasminogen. In this process, at day 2 after PQ exposure, TF initiated the exogenous coagulation pathway ($P=0.003$, Supplementary File), but no significant differences in TF expression levels were identified at day 7. In addition, antithrombin-III expression increased, thereby inhibiting coagulation pathway activity by inhibiting F10 and indirectly inhibiting C3 and C5 activity. Antithrombin-III, a key serine protease inhibitor in the plasma, regulates blood coagulation cascades [42]. During ALI, plasma antithrombin-III expression decreases, and exogenous antithrombin III not only inhibits over-activation of the coagulation pathway but also inhibits inflammatory responses [43]. Importantly, no prior studies have reported antithrombin-III expression in PQ-mediated ALI. Thus, we hypothesize that increased antithrombin-III levels might serve as a self-protection mechanism against PQ-induced lung injury.

Kininogen-1 inhibits thiol proteins and increased in expression at day 7 after PQ exposure. This protein promotes inflammatory responses, induces vasodilation, and increases capillary leakage by releasing the active peptide bradykinin [44]. A prior study has indicated significantly elevated total kininogen expression in the plasma and lung tissue of rats with chronic PQ poisoning, but no significant changes in high molecular weight (HMW) kininogen (73 kDa) [45]. In our study, HMW kininogen-1 was detected and verified, thus suggesting different roles of HMW kininogen-1 during PQ poisoning. Further research is necessary to determine the roles and mechanisms of HMW kininogen-1 and antithrombin-III during PQ-induced lung injury.

Interestingly, we identified two serine protease inhibitors: serpinA3N and serpinA3 M (subtype of SerpinA3). The protein levels of both proteases significantly increased at day 2 after PQ poisoning and were closely associated with complement and coagulation cascade pathway proteins. SerpinA3 is a plasma protease inhibitor synthesized in hepatocytes, bronchial epithelial cells, and neuronal cells [34, 35]. SerpinA3 inhibits several proteases in neutrophils and mast cells [32]. In

vitro investigations in mouse alveolar epithelial cells have shown that aprotinin (a serine protease inhibitor) decreases lung injury induced by influenza A virus [46]. However, few studies have investigated SerpinA3's roles in ALI. Accordingly, we hypothesized that in early PQ-induced ALI stages, elevated numbers of neutrophils gather in lung tissue and release serine proteases, thereby promoting further lung inflammation. High serpinA3 levels might function as a self-protection mechanism against excessive inflammation; however, the functions of the two subtypes of SerpinA3 (serpinA3N and serpinA3M) in PQ-induced lung injury warrant further study.

We also verified β-2-glycoprotein 1 (β2GPI), thrombospondin-1 (TSP-1), hemopexin, and serotransferrin proteins during PQ-induced lung injury. Importantly, these proteins are closely related to proteins in complement and coagulation cascade pathways. β2GPI binds several negatively charged molecules including phospholipids, dextran sulfate, and heparin. β2GPI has been reported to inhibit the intrinsic blood coagulation cascade via phospholipid interaction on damaged cell surfaces [47, 48]. In addition, β2GPI is one of three proteins (together with C-reactive protein and thrombomodulin) that, in the presence of external stimuli, dually up- and down-regulates complement and coagulation systems [49]. In addition, β2GPI is a key antigen in antiphospholipid syndrome, an autoimmune condition [50].

The extracellular glycoprotein TSP-1 has been implicated in inflammation and proliferation processes, and is highly elevated in activated platelets and stromal fibroblasts [51]. TSP-1 is associated with the regulation of collagen matrix formation, angiogenesis, platelet aggregation, and cell-matrix interactions during wound healing [52, 53]. Recently, TSP-1 has been reported to protect against *Pseudomonas aeruginosa*-induced lung injury [54]. Importantly, no studies to date have characterized the roles of β2GPI and TSP1 in PQ-induced lung injury. Whether the elevated expression of these proteins in early lung injury stages is protective or pathogenic remains unclear; therefore, further investigations are required.

Hemopexin and serotransferrin are involved in iron metabolism [55]; iron is transported by these proteins from absorption and heme degradation sites to storage and utilization locations. Elevated heme levels in lungs have been reported in ALI after insult, and hemopexin and serotransferrin putatively inactivate extracellular antioxidants' activity toward reactive heme-iron [56–58]. On the basis of our work and previous research, we hypothesize that hemopexin and serotransferrin might protect lung function against PQ exposure. Beyond their antioxidant roles, these molecules were observed to be closely associated with complement and coagulation cascade proteins, and thus might potentially serve as new therapeutic targets for PQ poisoning.

In summary, this study is the first, to our knowledge, to report significant changes in lung protein expression at various PQ induced lung injury stages in mice. Proteomics analyses identified several mechanisms underpinning PQ-mediated lung injury. PQ attacks alveolar/endothelial cells in lung tissues, thus resulting in the activation of immune responses. Severe lung damage is strongly dependent on over-activation of immune responses. Complement and coagulation cascades play critical roles during this process, particularly in early stages. The proteins identified in this study might serve as new therapeutic targets or biomarkers for PQ poisoning. However, further exploration is necessary to extend the data from this study.

Abbreviations

ALI	Acute lung injury
PQ	Paraquat
DEPs	Differentially expressed proteins
TMT	Tandem mass tag
LC-MS/MS	Liquid chromatography tandem mass spectrometry
PRM	Parallel reaction monitoring
H&E	Hematoxylin and eosin
CAN	Acetonitrile
HCD	High energy collisional dissociation
SVM	Support Vector Machine
GO	Gene ontology
KEGG	Kyoto Encyclopedia of Genes and Genomes
MF	Molecular function
BP	Biological process
CC	Cellular component
STRING	Search Tool for the Retrieval of Interacting Genes/Proteins
TLR-4	Toll-like receptor 4
MHC	Major histocompatibility complex
ARDS	Acute respiratory distress syndrome
DAMPs	Damage-associated molecular patterns
HIV	Human immunodeficiency virus
TF	Tissue factor
HMW	High molecular weight

Supplementary Information

The online version contains supplementary material available at https://doi.org/10.1186/s12931-024-03072-x.

Supplementary Material 1

Supplementary Material 2

Acknowledgements
Not applicable.

Author contributions
Wei Liu designed the study, Jinjin Peng, Yuqing Zhou and Liping Shan performed experiments. Liping Shan and Yuqing Zhou analyzed data. The manuscript was drafted and revised by Yuqing Zhou, Jinjin Peng and Liping Shan, and edited by Wei Liu. All authors approved the submitted work.

Funding
This research was supported by the National Natural Science Foundation of China (No. 81571882).

Data availability
No datasets were generated or analysed during the current study.

Declarations

Ethical approval
This study has been approved by the ethics committee of the First Hospital of China Medical University.

Consent for publication
Not applicable.

Competing interests
The authors declare no competing interests.

Received: 19 April 2024 / Accepted: 15 December 2024
Published online: 02 January 2025

References

1. Zyoud SH. Investigating global trends in paraquat intoxication research from 1962 to 2015 using bibliometric analysis. Am J Ind Med. 2018;61(6):462–70.
2. Gil H, Hong J, Jang S, et al. Diagnostic and therapeutic approach for acute paraquat intoxication. J Korean Med Sci. 2014;29(11):1441.
3. Chen F, Ye Y, Jin B, et al. Homicidal paraquat poisoning. J Forensic Sci. 2019;64(3):941–5.
4. Dinis-Oliveira RJ, Duarte JA, Sanchez-Navarro A, et al. Paraquat poisonings: mechanisms of lung toxicity, clinical features, and treatment. Crit Rev Toxicol. 2008;38(1):13–71.
5. Gawarammana IB, Buckley NA. Medical management of paraquat ingestion. Br J Clin Pharmacol. 2011;72(5):745–57.
6. Jiang WZ, Chen YQ, Zhang YL, et al. [Lung transplantation in patients with paraquat poisoning: a case report and literature review]. Zhonghua Lao Dong Wei Sheng Zhi Ye Bing Za Zhi. 2019;37(4):292–6.
7. Sørensen M, Loft S. No significant paraquat-induced oxidative DNA damage in rats. Free Radical Res. 2009;32(5):423–8.
8. Pei Y, Cai X, Chen J, et al. The role of p38 MAPK in acute paraquat-induced lung injury in rats. Inhal Toxicol. 2014;26(14):880–4.
9. Yang C, Song H, Liu W, et al. Protective effects of chymostatin on Paraquat-Induced acute lung injury in mice. Inflammation. 2017;41(1):122–33.
10. Ren M, Wang Y, Zhao J, et al. Metallothioneins attenuate paraquat-induced acute lung injury in mice through the mechanisms of anti-oxidation and anti-apoptosis. Food Chem Toxicol. 2014;73:140–7.
11. Li X, Wang W, Chen J. Recent progress in mass spectrometry proteomics for biomedical research. Sci China Life Sci. 2017;60(10):1093–113.
12. Zhang Z, Wu S, Stenoien DL, et al. High-throughput proteomics. Annu Rev Anal Chem. 2017;7(1):427–54.
13. Cao H, Zhu X, Chen X, et al. Quantitative proteomic analysis to identify differentially expressed proteins in the persistent atrial fibrillation using TMT coupled with nano-LC-MS/MS. Am J Transl Res. 2020;12(9):5032–47.
14. Liu B, Yin X, Wei H, et al. Quantitative proteomic analysis of rat retina with experimental autoimmune uveitis based on tandem mass tag (TMT) peptide labeling coupled with LC-MS/MS. J Chromatogr B. 2020;1153:122293.
15. Cho IK, Jeong M, You AS, et al. Pulmonary proteome and protein networks in response to the herbicide paraquat in rats. J Proteom Bioinform. 2015;8(5):67–79.
16. Dostal V, Wood SD, Thomas CT, et al. Proteomic signatures of acute oxidative stress response to paraquat in the mouse heart. Sci Rep. 2020;10(1):18440.
17. Venkatakrishnan P, Nakayasu ES, Almeida IC et al. Paraquat-Induced early phase changes in protein expression in whole tissue and mitochondria from rat liver. *The FASEB Journal*. 2009; 23:857.5-857.5.
18. Qian J, Liu L, Chen L, et al. Increased toll-like receptor 9 expression is associated with the severity of paraquat-induced lung injury in mice. Hum Exp Toxicol. 2015;34(4):430–8.
19. Matute-Bello G, Downey G, Moore BB, et al. An official American Thoracic Society workshop report: features and measurements of experimental acute lung injury in animals. Am J Respir Cell Mol Biol. 2011;44(5):725–38.
20. Wiśniewski JR, Zougman A, Nagaraj N, et al. Universal sample preparation method for proteome analysis. Nat Methods. 2011;6(5):359–62.
21. Yu C, Lin C, Hwang J. Predicting subcellular localization of proteins for Gram-negative bacteria by support vector machines based onn-peptide compositions. Protein Sci. 2004;13(5):1402–6.
22. Gotz S, Garcia-Gomez JM, Terol J, et al. High-throughput functional annotation and data mining with the Blast2GO suite. Nucleic Acids Res. 2008;36(10):3420–35.
23. Peterson AC, Russell JD, Bailey DJ, et al. Parallel reaction monitoring for high resolution and high mass accuracy quantitative, targeted proteomics. Mol Cell Proteom. 2012;11(11):1475–88.
24. MacLean B, Tomazela DM, Shulman N, et al. Skyline: an open source document editor for creating and analyzing targeted proteomics experiments. Bioinformatics. 2010;26(7):966–8.
25. Blanco-Ayala T, Anderica-Romero AC, Pedraza-Chaverri J. New insights into antioxidant strategies against paraquat toxicity. Free Radic Res. 2014;48(6):623–40.
26. Liu Z, Zhao H, Liu W, et al. NLRP3 inflammasome activation is essential for Paraquat-Induced acute lung injury. Inflammation. 2015;38(1):433–44.
27. Shen H, Wu N, Wang Y, et al. Toll-like receptor 9 mediates paraquat-induced acute lung injury: an in vitro and in vivo study. Life Sci. 2017;178:109–18.
28. Wang S, Zhu X, Xiong L, et al. Toll-like receptor 4 knockout alleviates paraquat-induced cardiomyocyte contractile dysfunction through an autophagy-dependent mechanism. Toxicol Lett. 2016;257:11–22.
29. Quevillon E, Silventoinen V, Pillai S, et al. InterProScan: protein domains identifier. Nucleic Acids Res. 2005;33:W116–20.
30. Su C, Jiang Y, Yang Y, et al. Responses of duckweed (Lemna minor L.) to aluminum stress: physiological and proteomics analyses. Ecotox Environ Safe. 2019;170:127–40.
31. Thompson A, Schäfer J, Kuhn K, et al. Tandem mass tags: a novel quantification strategy for comparative analysis of complex protein mixtures by MS/MS. Anal Chem. 2003;75(8):1895–904.
32. Xie J, Yan X, Xu G, et al. ITRAQ-based proteomics reveals the potential mechanism of fluoride-induced myocardial contraction function damage. Ecotox Environ Safe. 2020;197:110605.
33. Conigliaro P, Triggianese P, Ballanti E, et al. Complement, infection, and autoimmunity. Curr Opin Rheumatol. 2019;31(5):532–41.
34. Dostal V, Wood SD, Thomas CT, et al. Proteomic signatures of acute oxidative stress response to paraquat in the mouse heart. Sci Rep-Uk. 2020;10(1):18440.
35. Mihye Jeong IKC. Pulmonary proteome and protein networks in response to the herbicide paraquat in rats. J Proteom Bioinf. 2015;08(05):67–79.
36. Cui S, Nian Q, Chen G, et al. Ghrelin ameliorates A549 cell apoptosis caused by paraquat via p38-MAPK regulated mitochondrial apoptotic pathway. Toxicology. 2019;426:52267.
37. Wu Q, Xu Q, Jian X, et al. A new sight for paraquat poisoning from immunology. Immunopharm Immunot. 2018;40(4):269–72.
38. Lubbers R, van Essen MF, van Kooten C, et al. Production of complement components by cells of the immune system. Clin Exp Immunol. 2017;188(2):183–94.
39. Liszewski MK, Kolev M, Le Friec G, et al. Intracellular complement activation sustains T cell homeostasis and mediates effector differentiation. Immunity. 2013;39(6):1143–57.
40. Satyam A, Kannan L, Matsumoto N, et al. Intracellular activation of complement 3 is responsible for intestinal tissue damage during mesenteric ischemia. J Immunol. 2017;198(2):788–97.
41. Java A, Apicelli AJ, Liszewski MK et al. The complement system in COVID-19: friend and foe? JCI Insight. 2020; 5(15).
42. Allingstrup M, Wetterslev J, Ravn FB, et al. Antithrombin III for critically ill patients: a systematic review with meta-analysis and trial sequential analysis. Intens Care Med. 2016;42(4):505–20.
43. Sun HM, Hong LZ, Shen XK, et al. Antithrombin-III without concomitant heparin improves endotoxin-induced acute lung injury rats by inhibiting the activation of mitogen-activated protein kinase. Chin Med J (Engl). 2009;122(20):2466–71.
44. Maurer M, Bader M, Bas M, et al. New topics in bradykinin research. Allergy. 2011;66(11):1397–406.
45. Minakata K, Suzuki O, Oh Ishi S, et al. Acute-phase reactant proteins and antioxidants in rats intoxicated chronically with paraquat. J Toxicol Environ Health. 1995;44(1):29–41.
46. Song E, Españo E, Shim S, et al. Inhibitory effects of aprotinin on influenza a and B viruses in vitro and in vivo. Sci Rep-Uk. 2021;11(1):9427.
47. Miyakis S, Robertson SA, Krilis SA. Beta-2 glycoprotein I and its role in antiphospholipid syndrome—lessons from knockout mice. Clin Immunol. 2004;112(2):136–43.
48. Bertolaccini M, Sanna G. The clinical relevance of noncriteria antiphospholipid antibodies. Semin Thromb Hemost. 2018;44(05):453–7.

49. McDonnell T, Wincup C, Buchholz I, et al. The role of beta-2-glycoprotein I in health and disease associating structure with function: more than just APS. Blood Rev. 2020;3:100610–100610.
50. Serrano M, Martínez-Flores JA, Pérez D, et al. B2-Glycoprotein I/IgA Immune complexes. Circulation. 2017;135(20):1922–34.
51. Adams JC, Lawler J. The thrombospondins. Csh Perspect Biol. 2011;3(10):a009712–009712.
52. Bornstein P. Thrombospondins as matricellular modulators of cell function. J Clin Invest. 2001;107(8):929–34.
53. Sweetwyne MT, Murphy-Ullrich JE. Thrombospondin1 in tissue repair and fibrosis: TGF-beta-dependent and independent mechanisms. Matrix Biol. 2012;31(3):178–86.
54. Qu Y, Olonisakin T, Bain W et al. Thrombospondin-1 protects against pathogen-induced lung injury by limiting extracellular matrix proteolysis. JCI Insight. 2018; 3(3).
55. Johnson EE, Wessling-Resnick M. Iron metabolism and the innate immune response to infection. Microbes Infect. 2012;14(3):207–16.
56. Aggarwal S, Ahmad I, Lam A et al. Heme scavenging reduces pulmonary endoplasmic reticulum stress, fibrosis, and emphysema. *JCI insight*. 2018; 3(21).
57. Jung JY, Kwak YH, Chang I, et al. Protective effect of hemopexin on systemic inflammation and acute lung injury in an endotoxemia model. J Surg Res. 2017;212:15–21.
58. Ren Y, Smith A. Mechanism of metallothionein gene regulation by Heme-Hemopexin. J Biol Chem. 1995;270(41):23988–95.

Publisher's note